RP Materials: Proceedings (e-ISSN: 2583-8342)
Vol. 5, Part 1 (2026) pp. 214–223

RESEARCH PLATEAU PUBLISHERS

Cite this article: B. Kaur, K.K. Waraich, O.P. Pandey, Microstructural and thermo-physical evaluation of spontaneous fracture in automotive rear windshields: The role of carbonaceous impurity segregation, *RP Materials: Proceedings* Vol. 5, Part 1 (2026) pp. 214–223.

Original Research Article

Microstructural and thermo-physical evaluation of spontaneous fracture in automotive rear windshields: The role of carbonaceous impurity segregation

Bhupinder Kaur[1,*], Kamalpreet Kaur Waraich[2], O.P. Pandey[3]

[1]Department of Physics, Akal Degree College, Mastuana, Sangrur, 148001, India
[2]School of Arts & Sciences, American International University, Kuwait.
[3]School of Physics and Materials Science, Thapar Institute of Engineering & Technology, Patiala, 147001, India
[*]Corresponding author, E-mail: bhupinderkaursangrur@gmail.com

[**]Selection and Peer-Review under responsibility of the Scientific Committee of the 4th International Conference on Recent Trends in Materials Science & Devices 2026 (ICRTMD 2026) held at JVMGRR College, Charkhi Dadri, Haryana, India during 6–8 April 2026.

ARTICLE HISTORY
Received: 18 April 2026
Revised: 27 May 2026
Accepted: 27 May 2026
Published online: 24 June 2026

KEYWORDS
Automotive glass, Failure analysis, Carbonaceous impurities, Soda-lime-silica glass, Thermal stability.

ABSTRACT
This research investigates the spontaneous catastrophic failure of heavy-duty automotive rear windshields occurring under stable, shaded conditions. A multi-scale failure analysis was executed using dilatometry, differential thermal analysis (DTA), X-ray diffraction (XRD), scanning electron microscopy (SEM), and energy-dispersive X-ray spectroscopy (EDX). Microstructural characterization revealed carbonaceous impurities segregated into discrete banded structures within the soda-lime-silica matrix. These inclusions induce a significant coefficient of thermal expansion (CTE) mismatch, generating localized internal stress concentrations that trigger spontaneous crack propagation. Our findings conclusively link heterogeneous impurity distribution to the structural instability of the glass. This study provides a mechanistic framework for understanding impurity-induced fracture, offering critical insights for enhancing manufacturing quality control and automotive safety standards.

1. Introduction

Glass is a versatile material with countless applications, including its use in windshields [1]. Automotive windshields belong to the category of flat glass. The first glass windshields in automobiles debuted around 1905, coinciding with the invention of tempered glass. Tempering involves a special heat treatment that enhances the strength and durability of the glass, making it more resistant to shattering. Tempered glass windshields remained popular well into the mid-20th century. However, they were eventually replaced by laminated glass windshields, which consist of a multilayer unit with a plastic layer sandwiched between two sheets of glass. In many countries, including the U.S., the law mandates that auto windshields be made of laminated glass due to its safety features. Laminated glass combines the strength of tempered glass with the ability to flex slightly upon impact, providing additional protection against shattering. Nowadays, laminated glass is widely regarded as the safest option for auto glass. Its unique properties significantly reduce the risk of injury to the vehicle's passengers.

Glass consists of numerous oxides that fuse and react when heated. Windshield glass is primarily composed of several key components: silica sand (SiO_2), soda ash (Na_2CO_3), dolomite ($(CaMg)(CO_3)_2$), limestone ($CaCO_3$), and cullet [2]. Soda ash plays a crucial role in reducing the melting point of the glass batch composition [3]. Dolomite contributes to easier handling of the molten material, while limestone enhances the durability of the final product [4]. In addition to these primary components, small quantities of potassium oxide (K_2O), barium oxide (BaO), boric oxide (B_2O_3), titanium oxide (TiO_2), and aluminum oxide (Al_2O_3) are often incorporated to enhance glass crystallisation and photocatalytic properties, contributing to overall glass performance [5].

Most windshield glass is manufactured using the 'Float Method,' a name derived from the fact that the glass literally 'floats' inside a chamber during one of the manufacturing steps [6]. The process begins with the ingredients and water being mixed in a refractory tank, where they are subjected to very high temperatures and melted. The resulting molten mixture is then passed through a short but wide opening into a second tank known as the 'float chamber.' This chamber contains a thin layer of molten tin upon which the mixture floats, giving the process and chamber their names.

From this chamber, the long sheet of molten glass is transported on rollers into a specialised furnace, where it undergoes annealing. The annealed glass is then cut to the required dimensions using a diamond cutting tool called a 'scribe.' Following this, it is shaped and tempered, although this is not the final step. The glass sheet is placed onto or into a mold with the desired curvature and shape, heated until it becomes soft but doesn't melt, and then rapidly cooled by jets

of cold air. This tempering process significantly strengthens and hardens the glass [7], accompanied by development of surface compressive stress [8, 9].

Automobile windshield glass is typically exposed to harsh environmental conditions, including significant temperature fluctuations [10]. It is further heated by solar radiation [11]. Due to the glass's poor thermal conductivity, it develops non-uniform temperature distributions, leading to temperature gradients across the surface and within the glass. These gradients induce thermal stresses, which can be greatly exacerbated if the glass is suddenly exposed to cold water. The failures investigated in this study occurred under typical summer conditions in a region, where vehicles parked in the shade for several days (likely cooling to ambient temperature, around 25-35°C during summer nights) were subsequently exposed to hot sun (reaching 40-45°C or higher).

The manuscript serves as a case study of windshield glass failures reported to an automotive company to analyse the causes of glass failures during the use of vehicles.

2. Experimental

The impetus for this investigation arose from two distinct incidents of spontaneous rear windshield shattering in heavy-duty four-wheeler vehicles. In both cases, the failures occurred under similar environmental conditions. Specifically, the glass sheets shattered when the vehicles had been parked under a tree's shade for an extended period, approximately seven days, allowing the glass to cool down to ambient temperatures. The company reported that the glass subsequently shattered when the vehicle owners drove them in the daytime under the hot sun. Given the typical summer conditions in a region, where ambient temperatures can reach 25-35°C in the shade, and direct sunlight can heat surfaces to 40-45°C or higher, this scenario suggests a significant thermal shock. Consequently, the automotive company initiated a detailed failure analysis, sending samples of the broken glass granules from both incidents. To facilitate the analyses, these distinct glass samples were labeled as "S" and "X" glass, representing the two different models involved in the failures.

Table 1 provides a comparative overview of the chemical compositions of the commercial 'S' and 'X' glasses, which were used to manufacture the windshield sheets that experienced failure during vehicle operation.

Table 1: Glass composition (wt. %) with their label.

Constituents	S Glass	X Glass
SiO_2	72.46	72.46
Al_2O_3	1.23	1.23
CaO	9.23	9.23
MgO	2.23	2.23
Na_2CO_3	14.23	14.85
Synthetic Fe_2O_3	0.61	

While the overall chemical compositions of both the 'S' and 'X' glasses were largely consistent, minor yet significant variations were noted in their respective sodium carbonate (Na_2CO_3) and iron oxide (Fe_2O_3) content. These differences were of initial interest as Na_2CO_3 is a key component in reducing the melting point of glass, and variations could hint at different raw material sources. Specifically, the 'S' glass contained iron oxide as a deliberate tinting agent, imparting a slight colored effect to reduce light transmission into the car cabin. This tinting not only enhances the cooling effect but also effectively blocks infrared radiation [12]. The investigation proceeded with the comprehensive characterisation of these samples to understand the root cause of the failures.

To confirm the amorphous nature and structural integrity of the glasses, X-ray diffraction (XRD) analysis was performed using a Philips X'Pert Pro system from the Netherlands. The samples were scanned with a scan speed of 0.02°/min across a 2-theta range from 10° to 100°. Thermal behavior was meticulously investigated using Differential Thermal Analysis-Thermogravimetry (DTA-TG). Glass powder samples, weighing approximately 15 mg each, were subjected to DTA-TG in a nitrogen atmosphere using [platinum crucibles] at a differential heating rate of 10 °C/min, covering a temperature range from 50 °C to 1000 °C, with alumina serving as the reference material. The coefficient of thermal expansion for both glass types was accurately measured using a Netzsch DIL 402 PC dilatometer from the UK. Measurements were conducted at a heating rate of 5 °C/min in an air environment, typically spanning a temperature range from room temperature to 700°C.

Further detailed examination of the broken glass granules was carried out using a Scanning Electron Microscope (SEM, JEOL6400, Japan) in conjunction with Energy-Dispersive X-ray Spectroscopy (EDS). Before SEM/EDS analysis, the samples were coated with a thin layer of gold to ensure conductivity. EDS analysis was performed with an accelerating voltage of 15 kV or 20 kV to identify and map the elemental composition of the surface and fracture areas.

3. Results and discussion

The thermal decomposition and phase transitions of the glass samples were investigated using Differential Thermal Analysis (DTA) and Thermogravimetric Analysis (TGA). The DTA and TGA results for S and X glasses are presented in Figure 1(a) and 1(b), respectively.

For both glasses, the TGA curves show an initial weight loss up to approximately 200 °C (Region I), which is primarily attributed to the desorption of physically absorbed moisture. A more significant weight loss is observed between 200 °C and 400 °C (Region II) [13]. This weight loss is indicative of the presence of volatile components or the decomposition of bonded elements, possibly carbonaceous material, within the closed pores or as impurities within the glass structure. In the case of S glass (Figure 1(a)), a distinct weight gain is observed between 400 °C and 700 °C (Region III), which can be attributed to the oxidation of the iron (Fe) constituent, consistent with its known presence as a tinting agent [14]. Concurrently, the DTA curves reveal an exothermic peak around 450 °C for both S and X glasses, which strongly correlates with the burning off and oxidation of these carbonaceous impurities, providing further evidence of their presence within the glass matrix.

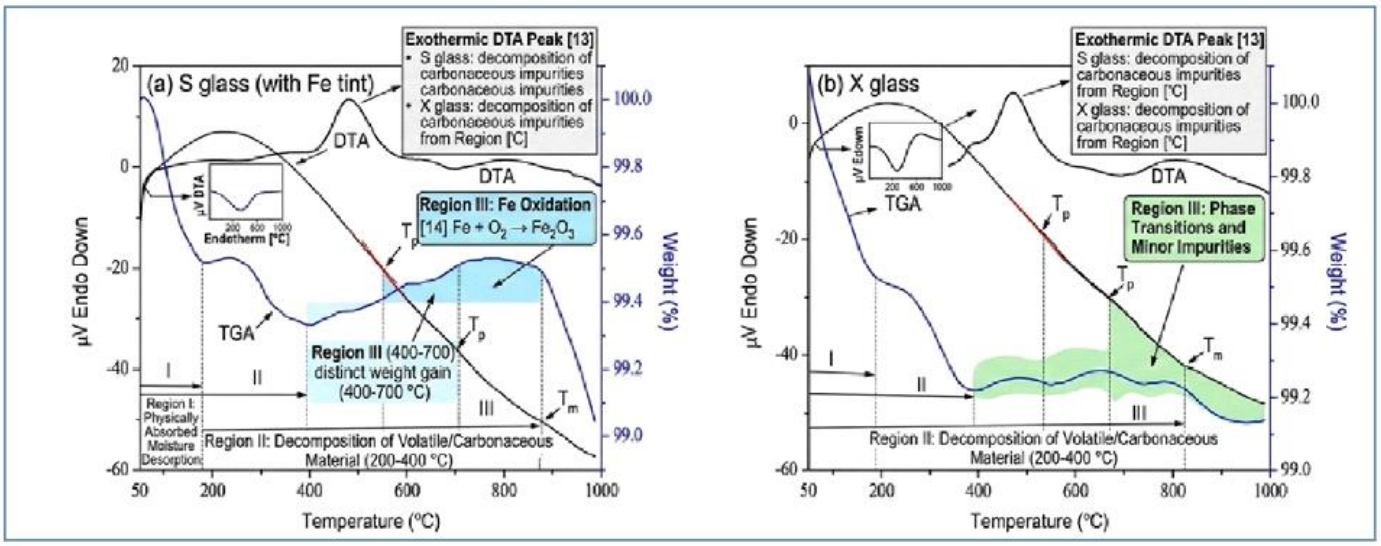

Figure 1: DTA and TGA analysis of (a) S glass and (b) X glass.

Figure 2 illustrates the thermal expansion behavior, specifically the variation in length relative to the original length (dL/dL_0), for both glass samples. Both S and X glasses generally exhibit a linear thermal expansion behavior with increasing temperature, as expected for amorphous materials, typically showing a coefficient of thermal expansion on the order of 10^{-6} K^{-1}. However, a careful and magnified analysis of the dilatometer curves in Figure 2(a) reveals subtle, microscopic kinks occurring between 200 °C and 400 °C [15]. While not confirmatory on its own, this behavior is highly symptomatic of localized internal stresses or microstructural changes. It suggests the possible presence of elements or inclusions within the glass matrix that possess a different coefficient of thermal expansion compared to the bulk glass. Upon heating, this thermal expansion mismatch can lead to localized detachment from the base matrix, potentially causing the formation of voids or localized stress concentrations within the glass. This initial observation provides a crucial symptomatic link to the presence of impurities that could influence the overall thermal stability and mechanical integrity of the windshield. The key thermal properties derived from these measurements, as observed in Figure 2(b), are comprehensively summarized in Table 2.

Table 2: Measured thermal properties of both glasses.

Glass Identity	T_g (°C)		T_s (°C)	TEC (10^{-6} K^{-1})
	From dilatometer	From DTA		
S Glass	550	555	580	8.0677×10^{-6}
X Glass	535	545	570	7.7278×10^{-6}

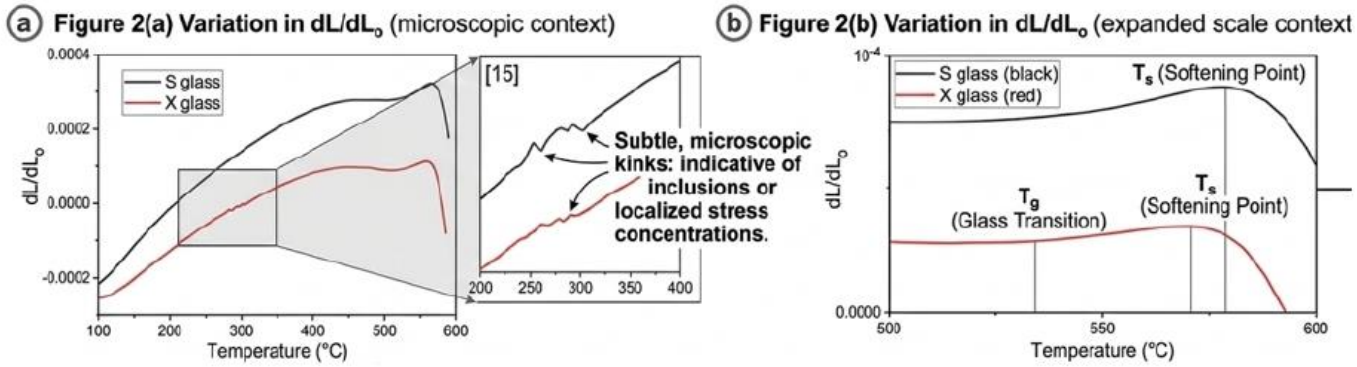

Figure 2: Variation in TEC values of (a) S glass and (b) X glass.

The structural characterization of both 'S' and 'X' glass samples was primarily performed using X-ray Diffraction (XRD) to confirm their amorphous state and assess their stability at various temperatures. As presented in Figure 3(a) and 3(b) for S and X glasses, respectively, the initial XRD patterns unequivocally confirmed the amorphous nature of both as-received glass samples, characterized by a broad, diffuse hump rather than sharp crystalline peaks.

To further evaluate their thermal stability and rule out any temperature-induced phase transformations that could contribute to fracture, the samples underwent controlled heat treatments. Each glass type was subjected to temperatures of 100 °C, 200 °C, 300 °C, 400 °C, and 600 °C for one hour. These heat-treated samples were then re-analyzed by XRD, denoted as S 100, S 200, S 300, S 400, and S 600 for the S glass series, and similarly for the X glass.

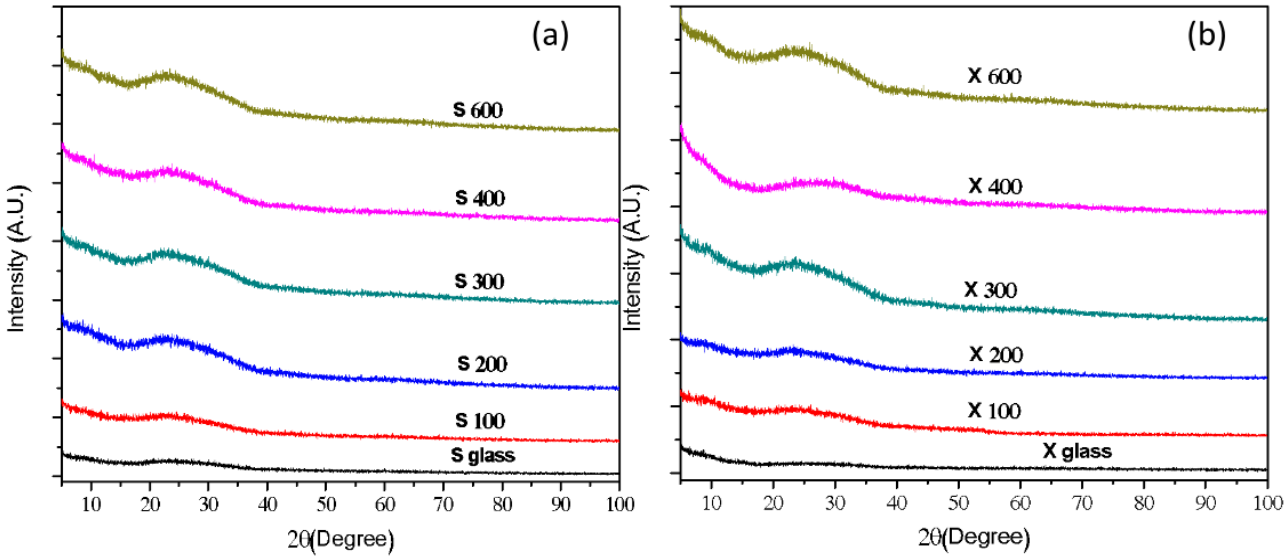

Figure 3: XRD pattern of as-received glasses and heat-treated windshield glasses showing amorphous characters.

Crucially, the XRD diffractograms of all heat-treated S and X glass samples, even those exposed to temperatures as high as 600 °C, consistently revealed the complete absence of any crystallized phases. The characteristic broad hump, a definitive indicator of an amorphous structure, remained prominently present in all analyzed samples. This robust analysis unequivocally demonstrates that the glass does not transform into a glass-ceramic or any other crystalline phase, even when subjected to significantly elevated temperatures within the operational range. Furthermore, it is important to note that this XRD analysis is sensitive enough to detect crystalline phases with a basic percentage exceeding 5%, thereby conclusively excluding the possibility of glass crystallization leading to the observed fractures in the windshields [16].

The spontaneous shattering of windshields in the specified conditions—where vehicles parked in shade are then exposed to direct sun—leads to rapid heating of the glass surface and subsequent heat transfer into the bulk material. To understand the microstructural features contributing to this failure, a meticulous microscopic analysis of the glass surfaces was essential, particularly using Scanning Electron Microscopy (SEM).

SEM analysis of the 'S' glass revealed significant heterogeneities across its surface, as depicted in Figure 4. Figure 4(a) highlights discrete inclusions observed in specific, localized areas, indicating non-uniformity in the glass matrix. Furthermore, Figure 4(b) shows that these inclusions were not isolated but often appeared in clusters within different regions, suggesting a pattern of impurity distribution rather than random occurrences. The visual characteristics of these light-colored inclusions strongly suggested the presence of carbonaceous material.

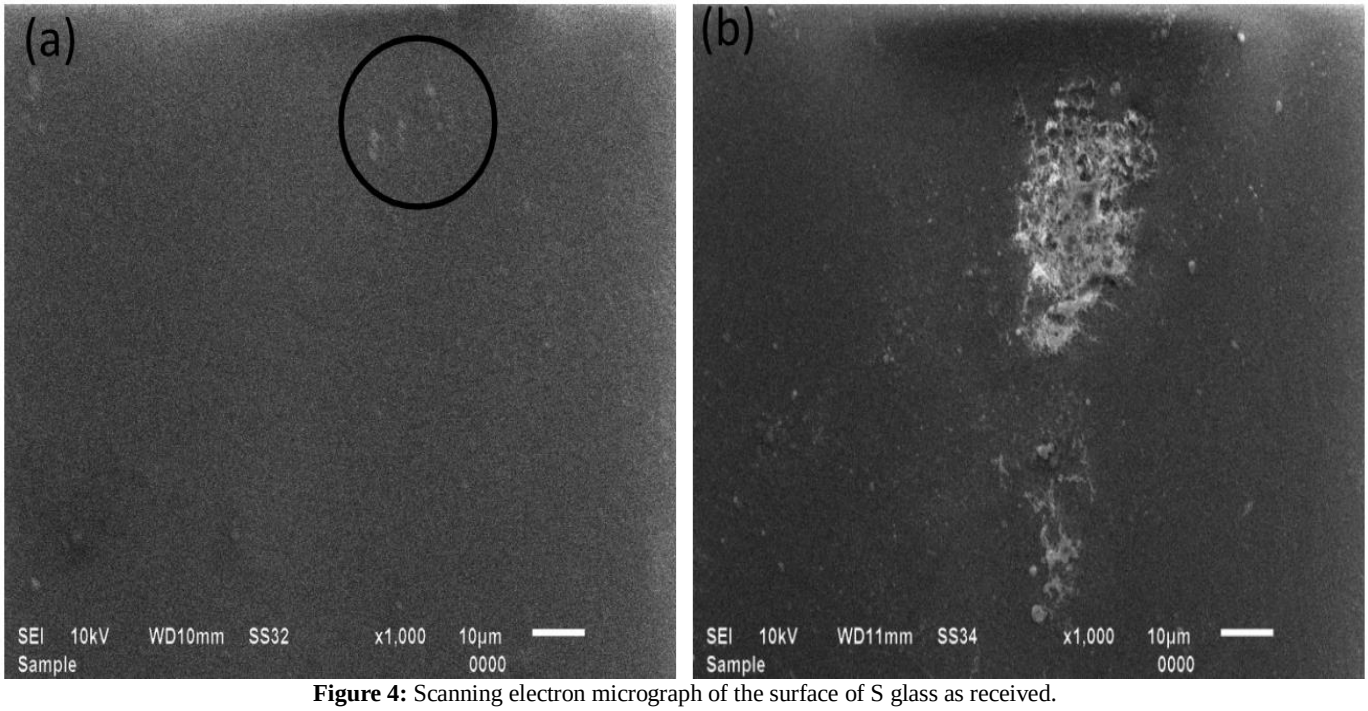

Figure 4: Scanning electron micrograph of the surface of S glass as received.

To definitively confirm the elemental composition of these inclusions, Energy-Dispersive X-ray Spectroscopy (EDS) analysis was performed by selecting specific areas on the glass surface. Figure 5 illustrates these selected areas for EDS investigation. Initially, a small area within a defined box was analyzed, as shown in Figure 5(a). The corresponding EDS spectra and elemental analysis (to be presented in a formalized Table 5 (a) indicated that this particular analyzed region was surprisingly devoid of carbon content, suggesting the heterogeneous nature of the inclusions.

However, a distinct zone, visually characterized by a prominent dark cavity, was subsequently analyzed as illustrated in Figure 5(b). This second, targeted EDS analysis unequivocally confirmed the presence of significant carbon content within the observed inclusions, as detailed in the corresponding elemental analysis (to be presented in a formalized Table 5(b). The observation of a dark cavity surrounding these carbon-rich areas is particularly significant. This morphology suggests that these carbon particles have preferentially occupied regions where solute rejection is at its maximum during the glass solidification process, typically occurring at the solid-liquid interface [17]. This phenomenon, often associated with solidification shrinkage, leads to the segregation of impurities like carbon into these localized areas, creating zones of compositional and structural inhomogeneity within the glass. These carbon-rich regions become critical points of weakness that can initiate fractures under thermal stress.

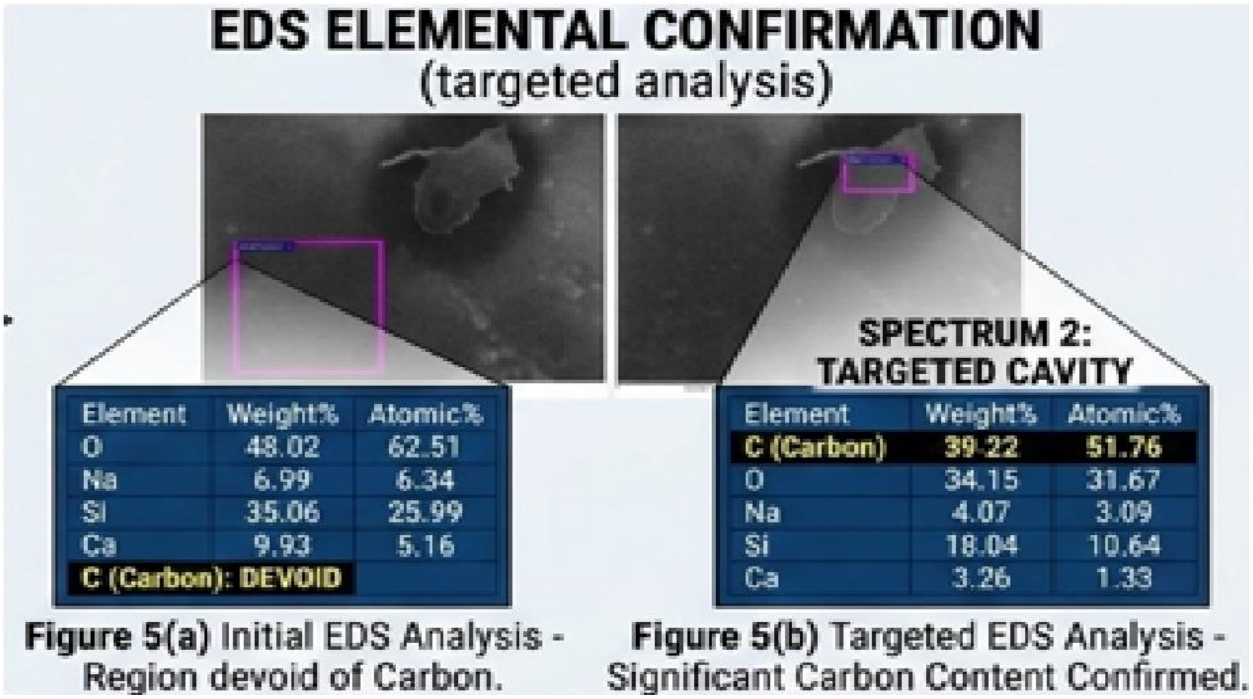

Figure 5: Back scattered electron micrograph with EDS analysis from the cleaned surface of S glass.

Figure 6 provides a compelling display of the topography within the fractured area of the S glass granules, offering critical insights into the underlying failure mechanism. The observed morphology distinctly indicates the pervasive presence of solidification shrinkage, a phenomenon inherent to the cooling and solidification of molten glass. This is unequivocally evidenced by the distinct, parallel shrinkage marks visible across the fractured surface. These marks are characteristic features formed when the molten glass contracts upon cooling, leading to the creation of internal cavities or voids within the solidifying matrix.

Crucially, within these intricate cavities and regions defined by solidification shrinkage, a significant segregation of carbon impurities was observed. This suggests that carbon, likely originating from raw material inconsistencies, preferentially accumulates in these areas of volume deficit during the glass manufacturing process. These structural anomalies, characterized by the presence of segregated carbon, typically begin to manifest at a depth of approximately 300 µm below the original glass surface. This depth indicates that these weaknesses are not merely superficial but extend into the bulk of the material, making the glass inherently vulnerable.

To provide definitive elemental confirmation of these impurity-rich zones, a targeted Energy-Dispersive X-ray Spectroscopy (EDS) analysis was conducted on specific areas within the fractured region, as visually illustrated by the box in Figure 7. The detailed elemental analysis from these highlighted regions, which should be comprehensively presented in an accompanying table, consistently revealed a significantly higher carbon content compared to the surrounding homogeneous glass matrix. This direct confirmation of carbon enrichment within the solidification shrinkage marks underscores these areas as critical points of compositional and structural inhomogeneity. The presence of these carbon-rich inclusions, with their distinct morphology and segregated nature, acts as a primary stress concentrator. Their inherently different coefficient of thermal expansion compared to the surrounding silicate glass leads to severe localized thermal stresses, particularly when the windshield undergoes rapid temperature fluctuations (e.g., from cooling in shade to direct exposure to hot sun), ultimately initiating and propagating cracks that result in the observed spontaneous shattering.

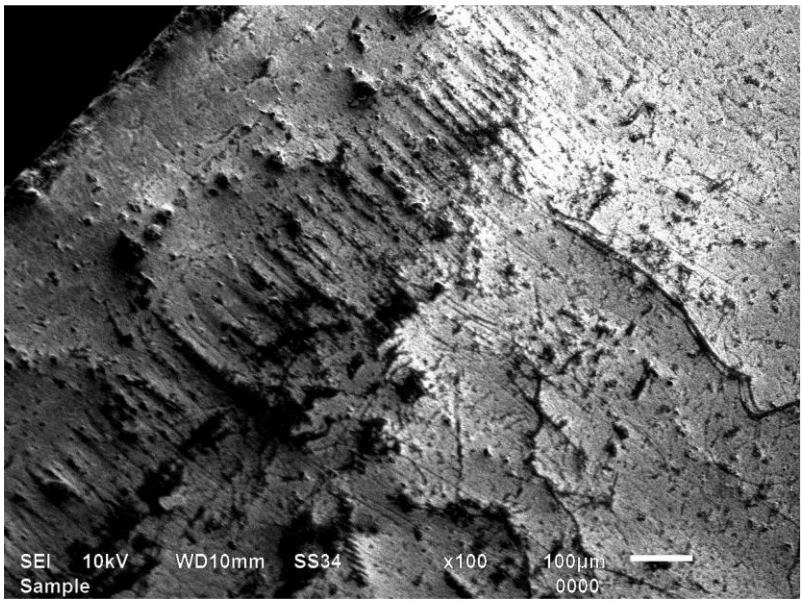

Figure 6: Scanning electron micrograph of the fractured area of S glass as received.

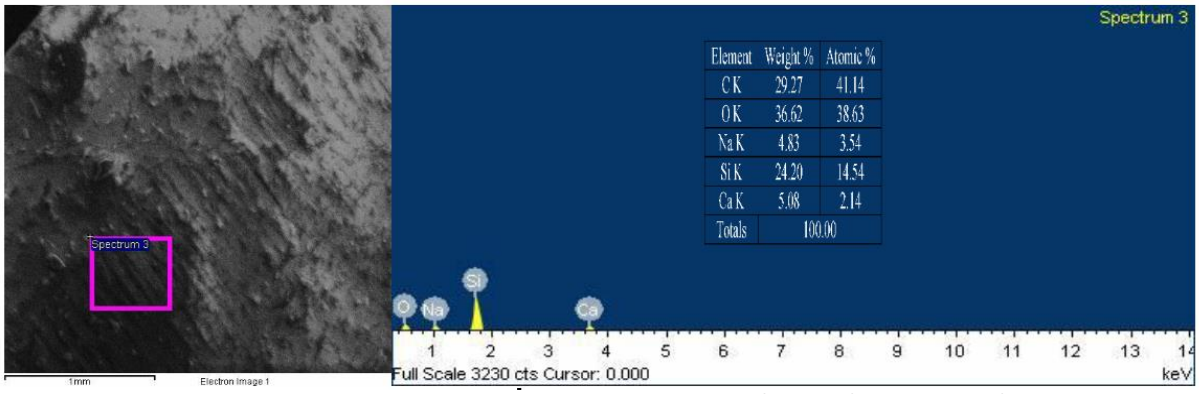

Figure 7: Back-scattered electron micrograph with EDS analysis from the fractured area of S glass.

Figure 8 presents a crucial SEM image of the X glass surface, revealing distinct microstructural features contributing to its failure. At various locations, the surface exhibits pronounced flow lines, indicative of inherent non-uniformities within the glass matrix, likely stemming from laminar flow patterns during the float manufacturing process. Concurrently, inclusions are consistently observed along these flow lines, distributed throughout the entire cross-section of the structure. This widespread presence creates a significantly heterogeneous microstructure, where undesirable heterogeneities are segregated, fundamentally compromising the uniformity and integrity glass.

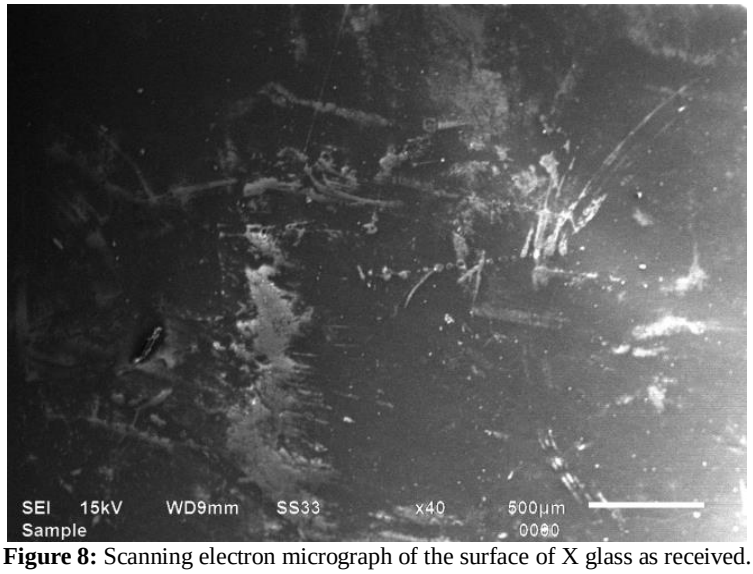

Figure 8: Scanning electron micrograph of the surface of X glass as received.

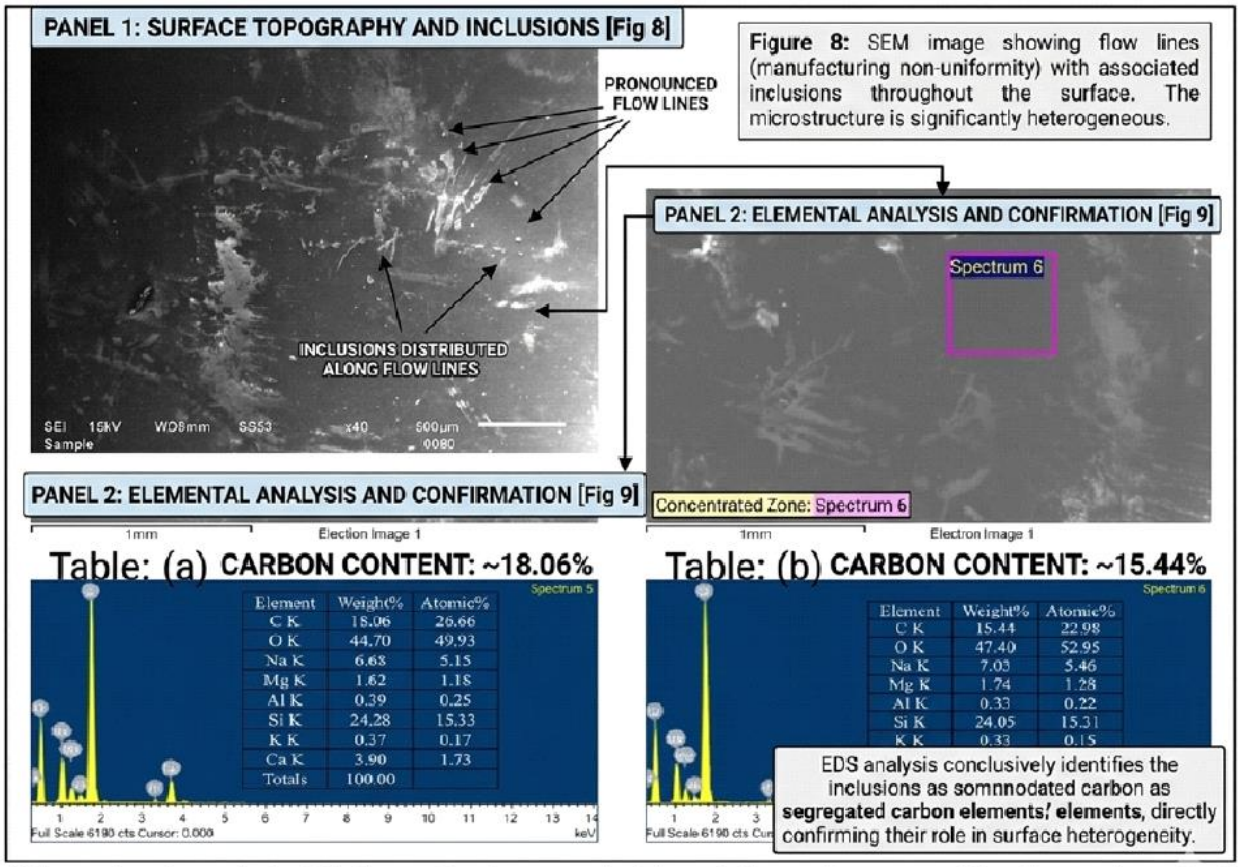

Figure 9: Back-scattered electron micrograph with EDS analysis from the surface of X glass.

Figure 8 presents a crucial SEM image of the X glass surface, revealing distinct microstructural features contributing to its failure. At various locations, the surface exhibits pronounced flow lines, indicative of inherent non-uniformities within the glass matrix, likely stemming from laminar flow patterns during the float manufacturing process. Concurrently, inclusions are consistently observed along these flow lines, distributed throughout the entire cross-section of the structure. This widespread presence creates a significantly heterogeneous microstructure, where undesirable heterogeneities are segregated, fundamentally compromising the glass's uniformity and integrity.

To conclusively identify the elemental composition of these heterogeneities, a focused Energy-Dispersive X-ray Spectroscopy (EDS) analysis was performed, as depicted in Figure 9. When the area under analysis was expanded to encompass regions containing both the bulk glass and these inclusions, the obtained carbon content measured approximately 18.0%, illustrated in Figure 9(a). Furthermore, a separate, more concentrated zone within the same area, illustrated in Figure 9(b), revealed an even higher carbon content, reaching up to 15.44%. These specific inclusions are unequivocally identified as carbon elements, confirming their direct role in the observed heterogeneity.

The systematic distribution of these carbon inclusions, particularly along flow lines and within areas of increased heterogeneity, strongly suggests a manufacturing-related origin. It appears highly probable that these glass fragments, rich in carbon inclusions, originate from the end portions of the last castings during the production process. These sections are typically more prone to such inhomogeneities and impurity segregation due to cooling dynamics and material flow patterns at the very end of the casting run. The pervasive presence and localized concentration of these carbon impurities, combined with their different thermal expansion coefficients compared to the surrounding glass, create inherent stress points that significantly reduce the overall strength and thermal shock resistance of the windshield, leading to its spontaneous shattering under thermal cycling.

Figure 10 provides a comprehensive representation of the entire cross-sectional area of the fractured surface of the X glass, offering critical insights into the internal distribution of impurities and the solidification process. In this micrograph, both ends of the cross-section distinctly exhibit a columnar drain structure, which manifests as prominent parallel lines extending inwards. Additionally, at the top and bottom regions of the cross-section, large clusters of inclusions are visibly segregated and prominently encircled, indicating significant areas of concentrated impurities.

This observation is highly consistent with the dynamics of glass solidification. During the cooling process, heat flows predominantly from the centre towards the surface of the solidifying glass. This directional heat release drives the fluid molten glass to move along these paths, effectively acting as conduits. Impurities, being less soluble or having different densities, tend to follow this path of fluid flow. As solidification progresses, these impurities become increasingly concentrated and ultimately get trapped within these columnar drain lines, forming the observed parallel structures.

Furthermore, in the central part of the cross-section, where solidification typically occurs last, solidification shrinkage is most pronounced. In these areas, the contracting glass creates larger voids and spaces, providing ample room for substantial "chunks" of impurities to segregate, which are encircled in Figure 10. These represent macroscopic accumulations of defects that profoundly compromise the glass's integrity.

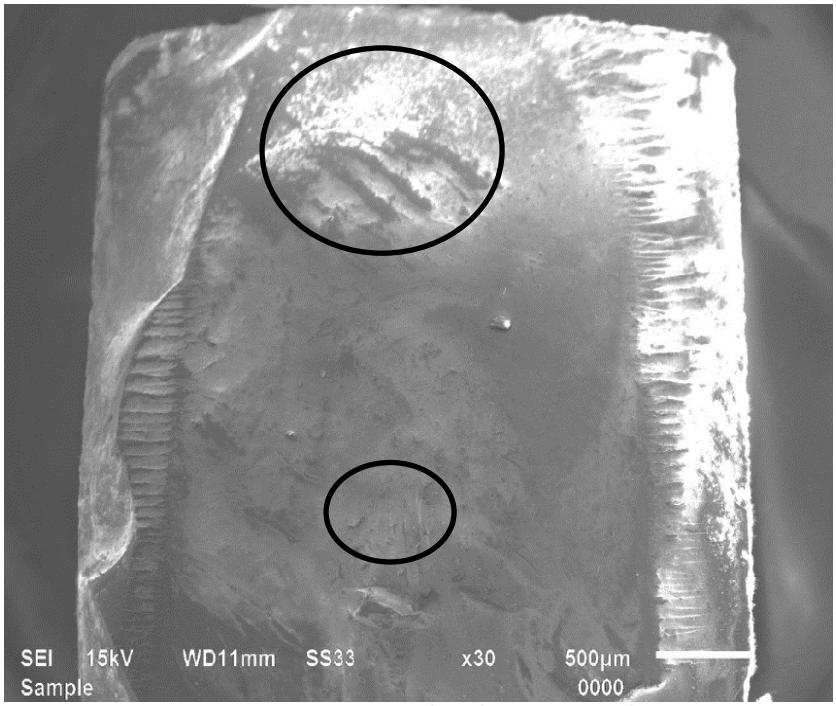

Figure 10: Scanning electron micrograph of the fractured area of X glass as received.

To confirm the elemental composition and concentration of these highly segregated impurities, a targeted Energy-Dispersive X-ray Spectroscopy (EDS) analysis was performed at one end of the cross-section, specifically focusing on a region where impurities were visibly aligned within the columnar drains. The precise area where this analysis was conducted is displayed in Figure 11. The results of this EDS analysis illustrate an exceptionally comprehensive view of carbon segregation, with its percentage amounting to a remarkably high 40.17%. This extremely elevated concentration of carbon, particularly within the columnar drain structures and large segregated clusters, definitively confirms that these impurities are carbonaceous. Their widespread distribution, high concentration, and entrapment within solidification features create significant internal inhomogeneities and localized stress concentrations, serving as the primary origin points for the thermal expansion mismatch that ultimately leads to the catastrophic shattering of the windshields.

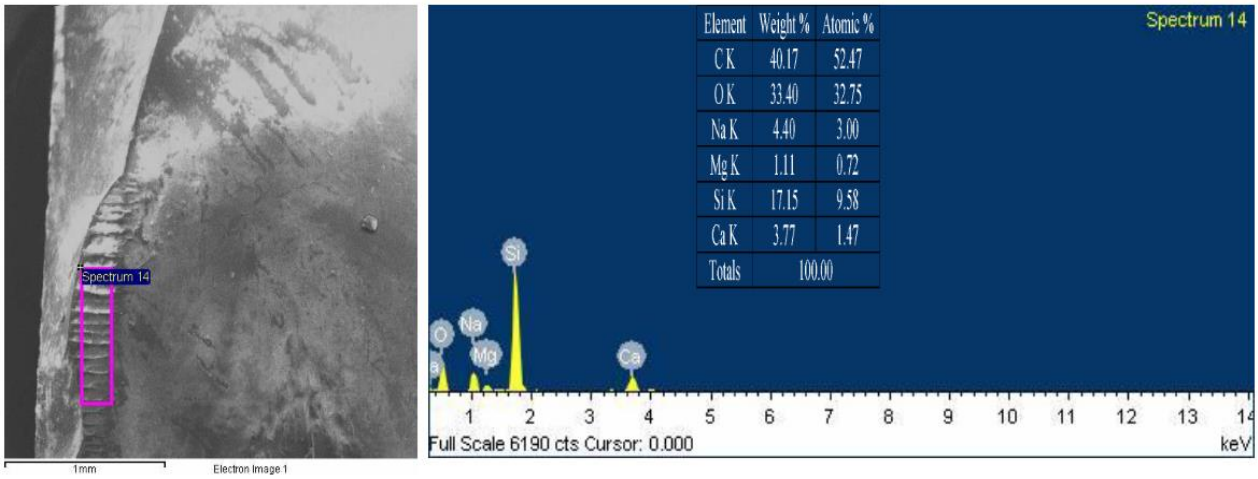

Figure 11: Back-scattered electron micrograph with EDS analysis from the fractured area of X glass.

The cumulative evidence from our multi-analytical investigation points definitively to the segregation of carbon impurities within the glass matrix as the predominant factor contributing to the observed spontaneous windshield failures. This carbon is not uniformly distributed but forms a distinct, often banded or drain-like structure within the glass, as extensively observed in the SEM micrographs.

When the windshields are exposed to direct solar radiation, these carbon-rich regions absorb a significantly higher amount of heat compared to the surrounding silicate

glass matrix. This differential heat absorption creates substantial localized thermal gradients within the glass structure. The critical consequence of this localized heating is a severe thermal expansion mismatch. Carbon possesses a significantly different coefficient of thermal expansion (CTE) compared to the soda-lime-silica glass. As the carbon inclusions heat up and attempt to expand at a rate different from the surrounding glass, immense internal tensile and compressive stresses are generated at the interfaces between the carbon impurities and the glass matrix [18].

Furthermore, the specific morphology of carbon segregation, particularly within the drain-like structures and larger segregated chunks (as observed in Figure 10), acts as a highly effective stress concentrator. These pre-existing defects, combined with the thermally induced stresses, render the glass inherently vulnerable. Even in the absence of a direct impact, the accumulated internal stresses can reach the fracture strength of the glass. This precarious state makes the windshield highly susceptible to shattering upon even slight external perturbations, such as minor mechanical shocks or vibrations experienced during normal vehicle movement, which would typically be harmless to an intact windshield. This vulnerability is strongly supported by comprehensive structural analysis and is consistent with the reported failure incidents [19]. Thus, the presence and specific distribution of carbon impurities directly compromise the thermal and mechanical integrity of the automotive glass.

4. Conclusions

The study reveals that the spontaneous shattering of automotive rear windshields is primarily due to the presence and segregation of carbon inclusions within the glass matrix. These carbon impurities are unevenly distributed and exist in various segregated forms, including distinct banded or drain-like structures.

The fundamental cause of failure stems from the non-uniform heat distribution that occurs when the vehicle's windshield is exposed to solar radiation. Carbon, possessing a significantly different absorption coefficient than glass, absorbs a substantially higher amount of incident heat. This differential absorption leads to the rapid development of severe localized thermal gradients, creating coexisting hot (carbon-rich) and cold (glass-rich) zones within the glass structure, often at close proximity, such as the observed 0.4 mm distance. This uneven heating, compounded by the differing coefficients of thermal expansion between carbon and glass, results in the generation of intense internal stresses. These inherent internal stresses represent a major pre-existing problem within the glass matrix, rendering the windshield highly susceptible to catastrophic failure upon even slight mechanical shocks, such as those induced by routine vehicle movement.

The failure is primarily a direct consequence of faulty raw materials used in the manufacturing process. The high concentration of carbon, which acts as the root cause of these failures, primarily originates from impurities within the soda ash used in the glass batch. This research emphasizes the need for stricter quality control measures on incoming raw materials, particularly soda ash, in automotive glass manufacturing. Addressing manufacturing-introduced inhomogeneities will improve the overall safety, reliability, and long-term durability of automotive glass components in service.

Acknowledgements

The authors gratefully acknowledge the financial support from UGC, India, under research grant nos. F. 4-1/2006 (BSR)/11-112/2008 (BSR) and F. 39-510/2010 (SR).

Authors' contributions

All authors contributed equally to the conception, design, experimental work, data analysis, interpretation of results, and preparation of the manuscript. All authors reviewed and approved the final version of the manuscript for publication.

Conflicts of interest

The author declares no conflict of interest.

Funding

This research received no external funding.

Data availability

No new data were created.

References

[1] A. Panait, Q.-C. He, B. Bary, M. Cossavella, K. Morcant, A coupled experimental and numerical approach to the integrity of friction-grip connections in glass structures, *Eng. Fail. Anal*. **14** (2007) 23–35.

[2] C.M. Bridge, J. Powell, K.L. Steele, M. Williams, J.M. MacInnis, M.E. Sigman, Characterization of automobile float glass with laser-induced breakdown spectroscopy and laser ablation inductively coupled plasma mass spectrometry, *Appl. Spectrosc*. **60** (2006) 1181–1187.

[3] E. Meechoowas, P. Ketboonruang, K. Tapasa, T. Jitwatcharakomol, Improve melting glass efficiency by batch-to-melt conversion, *Procedia Eng*. **32** (2012) 956–961.

[4] A. Nowak, M. Lubas, J.J. Jasinski, M. Szumera, R. Caban, J. Iwaszko, K. Koza, Effect of dolomite addition on the structure and properties of multicomponent amphibolite glasses, *Materials* (Basel) **15** (2022) 4870.

[5] P. Ponce-Peña, M.A. González-Lozano, M.Á. Escobedo-Bretado, D.M. Núñez-Ramírez, A. Rodríguez-Pulido, Z.V. Quiñones Jurado, M. Poisot, B. Sulbarán-Rangel, Crystallization of glasses containing K_2O, PbO, BaO, Al_2O_3, B_2O_3, and TiO_2, *Crystals* **12** (2022) 574.

[6] R.V. Kumar, J. Buckett, Float glass, *Ref. Module Mater. Sci. Mater. Eng*. (2017).

[7] K. Blank, Thermisch vorgespanntes Glas, *Glastech. Ber*. **52** (1979) 1.

[8] H. Gröber, S. Erk, U. Grigull, Die Grundgesetze der Wärmeübertragung, Springer-Verlag, Berlin/Heidelberg/New York (1981).

[9] W. Smetana, R. Reicher, Preventing failure of soda lime cover glasses by design optimization, *Eng. Fail. Anal*. **7** (2000) 87–99.

[10] C. Bousbaa, M. Kolli, M.A. Madjoubi, Z. Malou, T. Mahdaoui, N. Bouaouadja, Damage survey of a vehicle windshield exposed to sandblasting in Sahara, *Phys. Procedia* **2** (2009) 1141–1145.

[11] R. Kakade, P. Mer, Solar heat load on the vehicle occupants, *SAE Tech. Pap*. 2016-01-0246 (2016).

[12] M. Jacoby, Automotive glass presents unique challenges for manufacturing and recycling, *Inorg. Chem*. **100** (2022).

[13] S. Huang, Q. Lu, C. Wang, Y_2O_3–BaO–SiO_2–B_2O_3–Al_2O_3 glass sealant for solid oxide fuel cells, *J. Alloys Compd*. **509** (2011) 4348–4351.

[14] Review of the high-temperature oxidation of iron and carbon steels in air or oxygen, *Oxid. Met*. **59** (2003) 433–

468.
[15] H.-T. Chang, C.-K. Lin, C.-K. Liu, High-temperature mechanical properties of a glass sealant for solid oxide fuel cell, *J. Power Sources* **189** (2009) 1093–1099.
[16] A. Majumdar, S. Jana, Glass and glass–ceramic coatings, versatile materials for industrial and engineering applications, *Bull. Mater. Sci*. **24** (2001) 69–77.
[17] J.S. Sieger, Chemical characteristics of float glass surfaces, *J. Non-Cryst. Solids* **19** (1975) 213–220.
[18] G. Folena, S. Franz, F. Ricci-Tersenghi, Gradient descent dynamics in the mixed p-spin spherical model: finite-size simulations and comparison with mean-field integration, *J. Stat. Mech. Theory Exp.* **2021** (2021) 033302.
[19] M. Bergers, K. Natividad, S.M. Morse, et al., Full scale tests of heat strengthened glass with ceramic frit, *Glass Struct. Eng.* **1** (2016) 261–276.